

Quasinormal modes of Dirac field perturbation in Schwarzschild-anti-de Sitter black hole

Jiliang Jing*

*Institute of Physics and Department of Physics,
Hunan Normal University,
Changsha, Hunan 410081, P. R. China*

Abstract

The quasinormal modes (QNMs) associated with the decay of Dirac field perturbation around a Schwarzschild-anti-de Sitter (SAdS) black hole is investigated by using Horowitz-Hubeny approach. We find that both the real and the imaginary parts of the fundamental quasinormal frequencies for large black holes are linear functions of the Hawking temperature, and the real part of the fundamental quasinormal frequencies for intermediate and small black holes approximates a temperature curve and the corresponding imaginary part is almost a linear function of the black hole radius. The angular quantum number has the surprising effect of increasing the damping time scale and decreasing the oscillation time scale for intermediate and small black holes. We also find that the rates between quasinormal frequencies and black hole radii for large, intermediate and small black holes are linear functions of the overtone number, i. e., all the modes are evenly spaced.

PACS numbers: 04.70.-s, 04.50.+h, 11.15.-q, 11.25.Hf

*Electronic address: jljing@hunnu.edu.cn

I. INTRODUCTION

It is well known that the quasinormal modes (QNMs) of a black hole is defined as proper solutions of the perturbation equations belonging to certain complex characteristic frequencies which satisfy the boundary conditions appropriate for purely ingoing waves at the event horizon and purely outgoing waves at infinity [1]. The original interest in QNMs of black hole arose due to they are characteristics of black holes which do not depend on initial perturbations. It is generally believed that QNMs carry a unique footprint to directly identify the existence of a black hole. Through the QNMs, one can extract information about the physical parameters of the black hole—mass, electric charge, and angular momentum—from the gravitational wave signal by fitting the few lowest observed quasinormal frequencies to those calculated from the perturbation analysis, as well as test the stability of the event horizon against small perturbations. Recently, this interest has been renewed since the QNMs may be related to fundamental physics, such as the thermodynamic properties of black holes in loop quantum gravity [2] [3] since the real part of quasinormal frequencies with a large imaginary part for the scalar field in the Schwarzschild black hole is equal to the Barbero-Immirzi parameter [2][3][4][5], a factor introduced by hand in order that loop quantum gravity reproduces correctly the entropy of the black hole, and the QNMs of anti-de Sitter (AdS) black holes have a direction interpretation in terms of the dual conformal field theory (CFT) [6] [7] [8]. According to the AdS/CFT correspondence, a large static black hole in asymptotically AdS spacetime corresponds to a thermal state in CFT, and the decay of the test field in the black hole spacetime corresponds to the decay of the perturbed state in CFT. The dynamical timescale for the return to thermal equilibrium can be done in AdS spacetime, and then translated onto the CFT, using the AdS/CFT correspondence. It is quasinormal frequencies that give us the thermalization timescale which is very hard to compute directly. Therefore, many authors have delved into studies of QNMs associated with scalar, electromagnetic and gravitational perturbations in various asymptotically AdS black holes [9, 10, 11, 12, 13, 14, 15, 16, 17, 18].

Although much attention has been paid to the study of the QNMs for scalar, gravitational, electromagnetic field perturbations in the SAdS and the Reissner-Norström AdS black-hole backgrounds, however, to my best knowledge, at the moment the study of the QNMs for Dirac field perturbation in asymptotically AdS spacetime is still an open question. The main purpose of this paper is to study the QNMs associated with the decay of the Dirac field perturbation around a SAdS black hole.

The organization of this paper is as follows. In Sec. 2 the decoupled Dirac equations and corresponding wave equations in the SAdS spacetime are obtained by using Newman-Penrose formalism. In Sec. 3 the numerical approach to computing the Dirac QNMs is introduced. In

Sec. 4 the numerical results for the Dirac QNMs in the SAdS black hole are presented. Sec. 5 is devoted to a summary. In appendix we present the relations between our wave-equation and the standard one.

II. DIRAC EQUATIONS IN THE SCHWARZSCHILD-ANTI-DE SITTER SPACE-TIME

We begin with the SAdS metric

$$ds^2 = f dt^2 - \frac{1}{f} dr^2 - r^2(d\theta^2 + \sin^2\theta d\varphi^2), \quad (2.1)$$

with

$$f = 1 - \frac{2M}{r} + \frac{r^2}{R^2}, \quad (2.2)$$

where M represents the black hole mass, and R is the anti-de Sitter radius. Hereafter we will take $R = 1$ and measure everything in terms of R . The black hole horizon is located at r_+ , the largest root of the function f , and its Hawking temperature is given by

$$T_H = \frac{\kappa}{2\pi} = \frac{1}{4\pi} \left. \frac{df}{dr} \right|_{r_+} = \frac{3r_+^2 + 1}{4\pi r_+}, \quad (2.3)$$

where κ is a surface gravity. The mass parameter M can be viewed as a function of the horizon radius

$$M = \frac{r_+^3}{2} \left(1 + \frac{1}{r_+^2} \right). \quad (2.4)$$

The Dirac equations [19] are

$$\begin{aligned} \sqrt{2}\nabla_{BB'}P^B + i\mu\bar{Q}_{B'} &= 0, \\ \sqrt{2}\nabla_{BB'}Q^B + i\mu\bar{P}_{B'} &= 0, \end{aligned} \quad (2.5)$$

where $\nabla_{BB'}$ is covariant differentiation, P^B and Q^B are the two-component spinors representing the wave function, $\bar{P}_{B'}$ is the complex conjugate of P_B , and μ is the particle mass. In the Newman-Penrose formalism [20] the equations become

$$\begin{aligned} (D + \epsilon - \rho)P^0 + (\bar{\delta} + \pi - \alpha)P^1 &= 2^{-1/2}i\mu\bar{Q}^{1'}, \\ (\Delta + \mu - \gamma)P^1 + (\delta + \beta - \tau)P^0 &= -2^{-1/2}i\mu\bar{Q}^{0'}, \\ (D + \bar{\epsilon} - \bar{\rho})\bar{Q}^{0'} + (\delta + \bar{\pi} - \bar{\alpha})\bar{Q}^{1'} &= -2^{-1/2}i\mu P^1, \\ (\Delta + \bar{\mu} - \bar{\gamma})\bar{Q}^{1'} + (\bar{\delta} + \bar{\beta} - \bar{\tau})\bar{Q}^{0'} &= 2^{-1/2}i\mu P^0. \end{aligned} \quad (2.6)$$

For the SAdS spacetime (2.1) the null tetrad can be taken as

$$\begin{aligned}
l^\mu &= \left(\frac{r^2}{\Delta}, 1, 0, 0 \right), \\
n^\mu &= \frac{1}{2} \left(1, -\frac{\Delta}{r^2}, 0, 0 \right) \\
m^\mu &= \frac{1}{\sqrt{2}r} \left(0, 0, 1, \frac{i}{\sin\theta} \right),
\end{aligned} \tag{2.7}$$

with

$$\Delta = r^2 - 2Mr + r^4. \tag{2.8}$$

Then, if we set

$$\begin{aligned}
P^0 &= \frac{1}{r} f_1(r, \theta) e^{-i(\omega t - m\varphi)}, \\
P^1 &= f_2(r, \theta) e^{-i(\omega t - m\varphi)}, \\
\bar{Q}^{1'} &= g_1(r, \theta) e^{-i(\omega t - m\varphi)}, \\
\bar{Q}^{0'} &= -\frac{1}{r} g_2(r, \theta) e^{-i(\omega t - m\varphi)},
\end{aligned} \tag{2.9}$$

where ω and m are the energy and angular momentum of the Dirac particles, Eq. (2.6) can be simplified as

$$\begin{aligned}
\mathcal{D}_0 f_1 + \frac{1}{\sqrt{2}} \mathcal{L}_{1/2} f_2 &= \frac{1}{\sqrt{2}} i\mu r g_1, \\
\Delta \mathcal{D}_{1/2}^\dagger f_2 - \sqrt{2} \mathcal{L}_{1/2}^\dagger f_1 &= -\sqrt{2} i\mu r g_1, \\
\mathcal{D}_0 g_2 - \frac{1}{\sqrt{2}} \mathcal{L}_{1/2}^\dagger g_1 &= \frac{1}{\sqrt{2}} i\mu r f_2, \\
\Delta \mathcal{D}_{1/2}^\dagger g_1 + \sqrt{2} \mathcal{L}_{1/2} g_2 &= -\sqrt{2} i\mu r f_1,
\end{aligned} \tag{2.10}$$

with

$$\begin{aligned}
\mathcal{D}_n &= \frac{\partial}{\partial r} - \frac{iK}{\Delta} + \frac{n}{\Delta} \frac{d\Delta}{dr}, \\
\mathcal{D}_n^\dagger &= \frac{\partial}{\partial r} + \frac{iK}{\Delta} + \frac{n}{\Delta} \frac{d\Delta}{dr}, \\
\mathcal{L}_n &= \frac{\partial}{\partial \theta} + \frac{m}{\sin\theta} + n \cot\theta, \\
\mathcal{L}_n^\dagger &= \frac{\partial}{\partial \theta} - \frac{m}{\sin\theta} + n \cot\theta, \\
K &= r^2 \omega.
\end{aligned} \tag{2.11}$$

It is now apparent that the variables can be separated by the substitutions

$$\begin{aligned}
f_1 &= \mathbb{R}_{-1/2}(r)S_{-1/2}(\theta), \\
f_2 &= \mathbb{R}_{+1/2}(r)S_{+1/2}(\theta), \\
g_1 &= \mathbb{R}_{+1/2}(r)S_{-1/2}(\theta), \\
g_2 &= \mathbb{R}_{-1/2}(r)S_{+1/2}(\theta).
\end{aligned} \tag{2.12}$$

Then, Eq. (2.10) reduces to the following radial and angular parts

$$\sqrt{\Delta}\mathcal{D}_0\mathbb{R}_{-1/2} = (\lambda + i\mu r)\sqrt{\Delta}\mathbb{R}_{+1/2}, \tag{2.13}$$

$$\sqrt{\Delta}\mathcal{D}_0^\dagger(\sqrt{\Delta}\mathbb{R}_{+1/2}) = (\lambda - i\mu r)\mathbb{R}_{-1/2}, \tag{2.14}$$

$$\mathcal{L}_{1/2}S_{+1/2} = -\lambda S_{-1/2}, \tag{2.15}$$

$$\mathcal{L}_{1/2}^\dagger S_{-1/2} = \lambda S_{+1/2}. \tag{2.16}$$

We can eliminate $S_{+1/2}$ (or $S_{-1/2}$) from Eqs. (2.15) and (2.16) and obtain

$$\mathcal{L}_{1/2}^\dagger\mathcal{L}_{1/2}S_{+1/2} = -\lambda^2 S_{+1/2}, \tag{2.17}$$

$$\mathcal{L}_{1/2}\mathcal{L}_{1/2}^\dagger S_{-1/2} = -\lambda^2 S_{-1/2}. \tag{2.18}$$

Both them can be expressed as

$$\left[\frac{1}{\sin\theta} \frac{d}{d\theta} \left(\sin\theta \frac{d}{d\theta} \right) - \frac{m^2 + 2m\cos\theta + s^2\cos^2\theta}{\sin^2\theta} + s + A_s \right] S_s = 0, \tag{2.19}$$

here and hereafter we take $s = +1/2$ for the case $S_{+1/2}$ ($\mathbb{R}_{+1/2}$) and $s = -1/2$ for $S_{-1/2}$ ($\mathbb{R}_{-1/2}$), and $A_{+1/2} = \lambda^2 - 2s$ and $A_{-1/2} = \lambda^2$. The angular equation (2.19) can be solved exactly and $A_s = (l - s)(l + s + 1)$, where l is the quantum number characterizing the angular distribution. So, we have $\lambda^2 = (l + \frac{1}{2})^2$ for both cases $s = +1/2$ and $s = -1/2$.

In this paper we will focus our attention on the massless case. Then, we can eliminate $\mathbb{R}_{-1/2}$ (or $\sqrt{\Delta}\mathbb{R}_{+1/2}$) from Eqs. (2.13) and (2.14) to obtain a radial decoupled Dirac equation for $\sqrt{\Delta}\mathbb{R}_{+1/2}$ (or $\mathbb{R}_{-1/2}$), and we find that both them can be expressed as

$$\Delta^{-s} \frac{d}{dr} \left(\Delta^{1+s} \frac{d\mathbb{R}_s}{dr} \right) + P\mathbb{R}_s = 0, \tag{2.20}$$

with

$$P = \frac{K^2 - isK \frac{d\Delta}{dr}}{\Delta} + 4si\omega r + \frac{1}{2} \left(s + \frac{1}{2} \right) \frac{d^2\Delta}{dr^2} - \lambda^2, \tag{2.21}$$

We now try to express Eq. (2.20) as a wave-equation. Introducing an usual tortoise coordinate $dr_* = (r^2/\Delta)dr$ and resolving the equation in the form

$$\mathbb{R}_s = \frac{\Delta^{-s/2}}{r} \Psi_s, \tag{2.22}$$

then we obtain

$$\frac{d^2\Psi_s}{dr_*^2} + \left\{ \frac{dH}{dr_*} - H^2 + \frac{\Delta}{r^4} P \right\} \Psi_s = 0, \quad (2.23)$$

where

$$H = - \left[\frac{s}{2r^2} \frac{d\Delta}{dr} + \frac{\Delta}{r^3} \right]. \quad (2.24)$$

We find that Eq. (2.23) can be expressed as

$$\frac{d\Psi_s}{dr_*^2} + (\omega^2 - V)\Psi_s = 0, \quad (2.25)$$

where

$$V = -\frac{\Delta}{4r^2} \frac{d}{dr} \left[r^2 \frac{d}{dr} \left(\frac{\Delta}{r^4} \right) \right] + \frac{s^2 r^4}{4} \left[\frac{d}{dr} \left(\frac{\Delta}{r^4} \right) \right]^2 + i s \omega r^2 \frac{d}{dr} \left(\frac{\Delta}{r^4} \right) + \frac{\lambda^2 \Delta}{r^4}. \quad (2.26)$$

The potential V is complex and the complex frequency ω is not separated from V . We note that potentials which are functions of complex frequency have always been used to study QNMs in Refs. [21][22][23][24] because the key point to investigate QNMs is that we should get solutions of the original equations with appropriate boundary conditions presented in the introduction.

We should point out here that, for the Dirac fields, we can also obtain another two standard wave-equations $\left(\frac{d^2}{dr_*^2} + \omega^2 \right) Z_{\pm} = V_{\pm} Z_{\pm}$ with the potentials $V_{\pm} = \lambda^2 \frac{\Delta}{r^4} \pm \lambda \frac{d}{dr_*} \frac{\sqrt{\Delta}}{r^2}$ by using similar approach in Refs. [23][25][26]. At first sight the potentials are simpler than Eq. (2.26). However, if the Dirac quasinormal frequencies of the SAdS black hole are studied by using the potentials V_{\pm} and Horowitz-Hubeny approach[14], we find that we can not expand the potentials about the event horizon r_+ due to the potentials include a non-polynomial factor $\sqrt{\Delta}$. Although we can expand them about $y = 0$ with $y^2 = r - r_+$, the expansion function will be an infinite series. Therefore, the numerical calculation will take very long computer time to get Dirac fundamental quasinormal frequencies, and it is very difficult to find higher overtone modes. On the other hand, in appendix we present the relations between the two kinds of the wave functions in our wave-equation and the standard one which imply that the quasinormal frequencies are the same for both cases. These are the reasons why we use the potential (2.26) to study Dirac QNMs of the SAdS black hole here.

III. NUMERICAL APPROACH TO COMPUTING DIRAC QUASINORMAL MODES

For the SAdS black hole, the potential (2.26) diverges at infinity, so we must require that Ψ_s vanish there. QNMs are defined to be modes with only ingoing waves near the event horizon.

The boundary conditions on wave function Ψ_s (or \mathbb{R}_s) at the horizon ($r = r_+$) and infinity ($r \rightarrow +\infty$) can be expressed mathematically as

$$\Psi_s \sim \Delta^{s/2} \mathbb{R}_s \sim \begin{cases} \Delta^{-s/2} e^{-i\omega r_*} & r \rightarrow r_+, \\ 0 & r \rightarrow +\infty. \end{cases} \quad (3.1)$$

Equations (2.25), (2.26) and (3.1) determine an eigenvalue problem for the quasinormal frequency ω of the Dirac field perturbation.

In what follows, we will calculate the quasinormal frequencies for outgoing Dirac field (i.e., for case $s = -1/2$ [21]) by using the Horowitz-Hubeny approach [14]. Writing Φ_s for a generic wave function as

$$\Phi_s = \Psi_s e^{i\omega r_*}, \quad (3.2)$$

we find that Eq. (2.25) can be rewritten as

$$f^2 \frac{d^2 \Phi_s}{dr^2} + \left(f \frac{df}{dr} - 2i\omega f \right) \frac{d\Phi_s}{dr} - V \Phi_s = 0. \quad (3.3)$$

In order to map the entire region of interest, $r_+ < r < +\infty$, into a finite parameter range, we change variable to $x = 1/r$. Define a new function $B(x)$ as

$$B(x) = x^2 - \frac{1 + x_+^2}{x_+^3} x^3 + 1, \quad (3.4)$$

then f can be rescaled as

$$f = x^2 \Delta = \frac{B(x)}{x^2}. \quad (3.5)$$

In terms of the new variable x , Eq. (3.3) can be expressed as

$$S(x) \frac{d^2 \Phi_s}{dx^2} + \frac{T(x)}{x - x_+} \frac{d\Phi_s}{dx} + \frac{U(x)}{(x - x_+)^2} \Phi_s = 0, \quad (3.6)$$

where the coefficient functions are described as

$$\begin{aligned} S(x) &= \frac{B(x)^2}{(x - x_+)^2} = \left(\frac{1 + x_+^2}{x_+^3} x^2 + \frac{x}{x_+^2} + \frac{1}{x_+} \right)^2, \\ T(x) &= \frac{B(x)}{x - x_+} \left(\frac{dB(x)}{dx} + 2I\omega \right) = \left(\frac{1 + x_+^2}{x_+^3} x^2 + \frac{x}{x_+^2} + \frac{1}{x_+} \right) \left(\frac{3(1 + x_+^2)}{x_+^3} x^2 - 2x - 2I\omega \right), \\ U(x) &= -V = \frac{B(x)}{4} \frac{d^2 B(x)}{dx^2} - \frac{s^2}{4} \left(\frac{dB(x)}{dx} \right)^2 + is\omega \frac{dB(x)}{dx} - \lambda^2 B(x). \end{aligned} \quad (3.7)$$

Since $S(x)$, $T(x)$ and $U(x)$ are all polynomial of degree 4, we can expand them about the horizon $x = x_+$ as $S(x) = \sum_{n=0}^4 S_n (x - x_+)^n$, and similarly for $T(x)$ and $U(x)$.

To evaluate quasinormal frequencies by using Horowitz-Hubeny method, we need to expand the solution to the wave function Φ_s around x_+ ,

$$\Phi_s = (x - x_+)^\alpha \sum_{k=0}^{\infty} a_k (x - x_+)^k, \quad (3.8)$$

and to find the roots of the equation $\Phi_s|_{x=0} = 0$. First, we should determine the behavior of the solutions near the black hole horizon. Then, we should substitute Eq. (3.8) into the differential equation (3.6) in order to get a recursion relation for a_k . At last, we have to look for some true root which is the sought quasinormal frequency.

To find index α we set $\Phi_s = (x - x_+)^\alpha$ near the event horizon and substitute it into Eq. (3.6). Then, we have

$$\alpha(\alpha - 1)S_0 + \alpha T_0 + U_0 = 4\alpha\kappa(\alpha\kappa - i\omega) - 2s\kappa\left(\frac{s}{2}\kappa + i\omega\right) = 0, \quad (3.9)$$

which has two solutions $\alpha = -\frac{s}{2}$ and $\alpha = \frac{s}{2} + \frac{i\omega}{\kappa}$. Since we need only ingoing modes near the event horizon, that is to say, Φ_s must satisfy the boundary condition (3.1), we take $\alpha = -\frac{s}{2}$. Then Φ_s is described by

$$\Phi_s = (x - x_+)^{-s/2} \sum_{k=0}^{\infty} a_k (x - x_+)^k. \quad (3.10)$$

Substituting Eq. (3.10) into Eq. (3.6) we find the following recursion relation for a_n

$$a_n = -\frac{1}{Z_n} \sum_{k=0}^{n-1} \left[\left(k - \frac{s}{2}\right) \left(k - \frac{s}{2} - 1\right) S_{n-k} + \left(k - \frac{s}{2}\right) T_{n-k} + U_{n-k} \right] a_k, \quad (3.11)$$

where

$$Z_n = 4n\kappa[(n - s)\kappa - i\omega]. \quad (3.12)$$

The boundary condition (3.1) at $r \rightarrow \infty$ is now becomes

$$\Phi_s = (x - x_+)^{-s/2} \sum_{k=0}^{\infty} a_k (x - x_+)^k \rightarrow 0, \quad (3.13)$$

as $x \rightarrow 0$. Taking the limit of the equation we get

$$\sum_{k=0}^{\infty} a_k (-x_+)^k = 0. \quad (3.14)$$

The computation of quasinormal frequencies is now reduced to that of finding a numerical solution of the Eq. (3.14). We first truncate the sum (3.14) at some large $k = N$ and then check that for greater k (say 40 larger than N) the roots converge to some true roots, i.e.,

quasinormal frequencies. In the series (3.11) and (3.14) each next term depends on all the preceding terms through the recursion relations, and the roots of (3.14) suffer a sharp change for a small change on any of the input parameters, especially for finding higher overtone modes. In order to avoid the “noisy” we increase the precision of all the input data and we retain 50-digital precision in all the intermediate process. We find that the 50-digital precision is necessary because we have checked that, for $r_+ = 100$ and $N = 400$, 20-digital precision gives 4 convergent roots, 40-digital precision shows 9 convergent roots and 50-digital precision presents 11 convergent roots.

IV. NUMERICAL RESULTS FOR DIRAC QUASINORMAL FREQUENCIES

In this section, we will represent the numerical results obtained by using the numerical procedure just outlined in the previous section. The results will be organized into four subsections: the fundamental QNMs (the overtone number $n = 0$ and the size of black hole run from $r_+ = 0.4$ to $r_+ = 100$), large black holes ($r_+ = 1000$ and $r_+ = 100$), an intermediate black hole ($r_+ = 1$), and a small black hole ($r_+ = 0.4$) QNMs (the overtone number runs from $n = 0$ to $n = 10$).

A. Fundamental Quasinormal Modes

The fundamental quasinormal frequencies ($n = 0$) corresponding to $\lambda = 1$ Dirac perturbation of the SAdS black hole are given by table (I) and corresponding results are drawn in Fig. (1) for large black holes and in Fig. (2) for intermediate and small black holes. From the table and figures we find that, for large black holes, both the real and the imaginary parts of the quasinormal frequency are linear functions of the Hawking temperature, and the lines are described by

$$Re(\omega) = 8.367T, \tag{4.1}$$

$$- Im(\omega) = 6.371T. \tag{4.2}$$

The Fig. (2) shows that, for intermediate and small size black holes, the quasinormal frequencies do not scale with the Hawking temperature. Here $Re(\omega)$ approximates the temperature T more closely than the black hole size r_+ , but it is not diverging for small black holes. However, for $Im(\omega)$, the points continue to lie along (the points for black holes with radius $r_+ \leq 1.5$ lie

TABLE I: The fundamental quasinormal frequencies ($n = 0$) corresponding to $\lambda = 1$ Dirac perturbation of the SAdS black hole.

r_+	$\text{Re}(\omega)$	$-\text{Im}(\omega)$	r_+	$\text{Re}(\omega)$	$-\text{Im}(\omega)$
100	199.769	152.016	2.5	5.3747	3.6959
75	149.834	114.012	2	4.4620	2.9113
50	99.8993	76.0043	1.5	3.5961	2.1126
25	49.9795	37.9952	1	2.8219	1.2836
10	20.0744	15.1751	0.8	2.5596	0.9348
5	0.1834	7.5476	0.6	2.3439	0.5677
3.5	7.2683	5.2449	0.4	2.2045	0.1714
3	6.3135	4.4727			

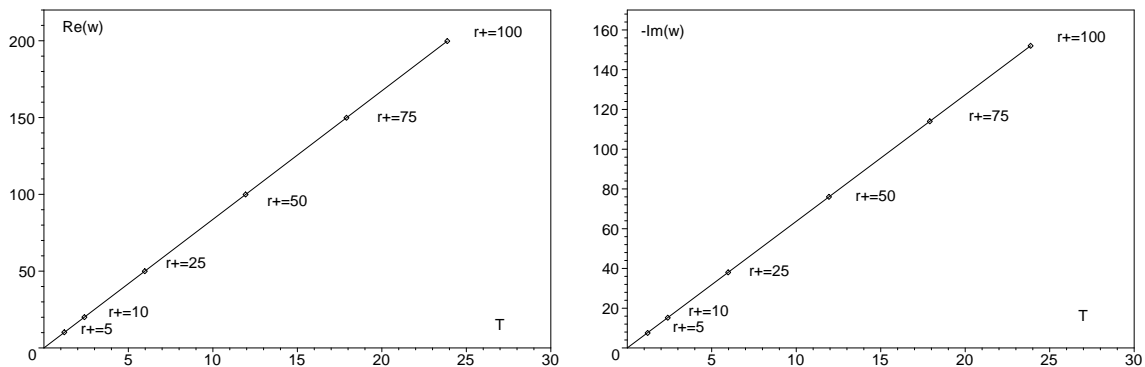


FIG. 1: Graphs of fundamental quasinormal frequencies ω versus Hawking temperature T for large black holes. The left figure is drawn for the cases $\text{Re}(\omega)$ and right one for $\text{Im}(\omega)$. The figures show that both the real and the imaginary parts of the frequency are linear function of T , and the lines are described by $\text{Re}(\omega) = 8.367T$ and $-\text{Im}(\omega) = 6.371T$.

slightly off) a straight line

$$-\text{Im}(\omega) = 1.499r_+. \quad (4.3)$$

We also study the relation between the quasinormal frequencies and the angular quantum number and find that, for large black hole (say $r_+ = 100$), the quasinormal frequencies depend very weakly on the low angular quantum number (say $l = 3/2$ and $l = 5/2$). However, for intermediate black hole ($r_+ = 1$), Fig (3) shows that the angular quantum number l mode has the surprising effect of decreasing $|\text{Im}(\omega)|$ (increasing the damping time scale) and

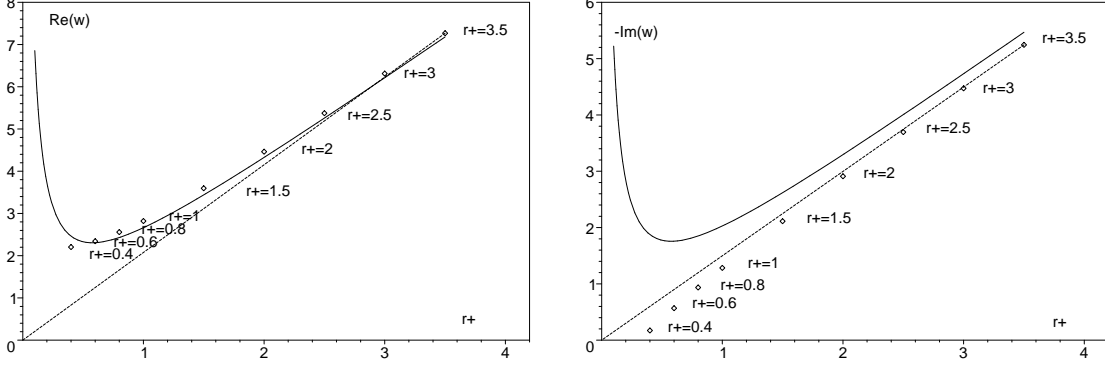


FIG. 2: $Re(\omega)$ and $Im(\omega)$ of the fundamental quasinormal frequencies versus radius r_+ for intermediate and small black holes. The dashed lines are $Re(\omega) = 2.706r_+$ in the left figure and $-Im(\omega) = 1.499r_+$ in the right one, and the solid lines are $Re(\omega) = 8.367T$ in the left figure and $-Im(\omega) = 6.371T$ in the right one.

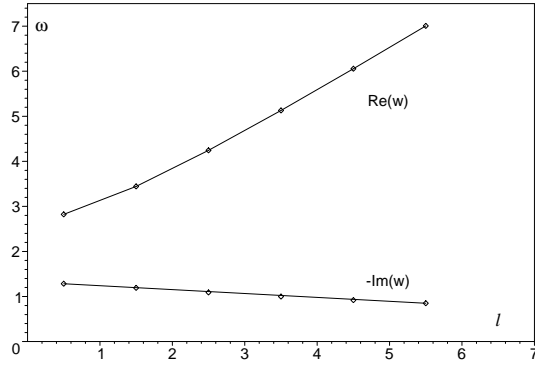


FIG. 3: Dependence of the fundamental quasinormal frequencies ω on the angular quantum number l for an intermediate SAdS black hole ($r_+ = 1$), which shows that l has the surprising effect of decreasing $|Im(\omega)|$ and increasing $Re(\omega)$.

increasing $Re(\omega)$ (decreasing the oscillation time scale). We have checked that the result for the intermediate black hole is also valid for the small black holes.

B. Quasinormal Modes for Large black holes

We show in Table (II) and Fig (4) the quasinormal frequencies corresponding to $\lambda = 1$ Dirac perturbation of large SAdS black holes ($r_+ = 1000$ and $r_+ = 100$). Perhaps the most interesting result for these large black holes is that the points for each overtone modes in Fig. (4) continue to lie along the straight lines $\frac{Re(\omega(n))}{r_+} = 1.35n + 2.136$ and $\frac{Im(\omega(n))}{r_+} = -(2.25n + 1.50)$. We have

TABLE II: Quasinormal frequencies corresponding to $\lambda = 1$ Dirac perturbation of large SAdS black holes ($r_+ = 1000$, $r_+ = 100$).

$r_+ = 1000$			$r_+ = 100$	
n	$\text{Re}(\omega)$	$-\text{Im}(\omega)$	$\text{Re}(\omega)$	$-\text{Im}(\omega)$
0	1997.59	1520.19	199.769	152.016
1	3505.31	3705.82	350.548	370.580
2	4923.53	5909.28	492.377	590.927
3	6305.63	8123.53	630.595	812.353
4	7668.35	10344.6	766.875	1034.46
5	9019.10	12570.3	901.947	1257.03
6	10361.4	14799.3	1036.20	1479.94
7	11697.8	17030.9	1169.85	1703.10
8	13029.8	19264.5	1303.05	1926.45
9	14358.2	21499.7	1435.90	2149.98
10	15896.7	23802.2	1601.11	2371.15

checked that the behave of the QNMs can be described as

$$\frac{\omega(n)}{r_+} \sim (1.35 - 2.25i)n + (2.136 - 1.500i) \quad (4.4)$$

with an error of about 2%. This leads to the spacing

$$\frac{\omega_{(n+1)} - \omega_{(n)}}{r_+} = (1.35 - 2.25i). \quad (4.5)$$

C. Quasinormal Modes for intermediate size black hole

In Table (III) and Fig. (5) we show some of the quasinormal frequencies corresponding to $\lambda = 1$ Dirac perturbation of an intermediate black hole ($r_+ = 1$). We find again that the points for each overtone modes continue to lie along the straight lines $\frac{\text{Re}(\omega(n))}{r_+} = 2.02n + 2.86$ and $\frac{\text{Im}(\omega(n))}{r_+} = -(2.32n + 1.26)$, i. e., the behave of the QNMs can be expressed as

$$\frac{\omega(n)}{r_+} \sim (2.02 - 2.32i)n + (2.86 - 1.26i) \quad (4.6)$$

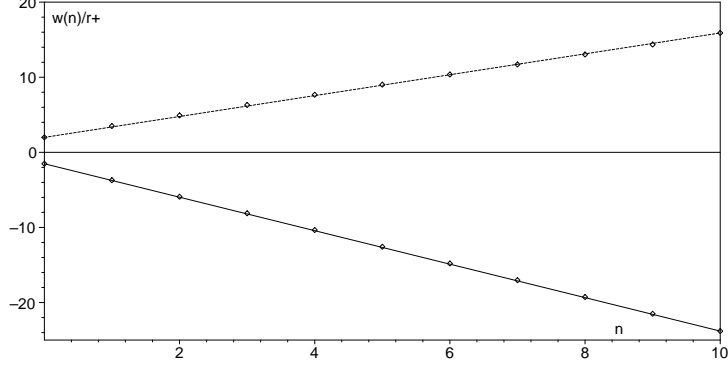


FIG. 4: $\frac{\omega(n)}{r_+}$ versus overtone number n for large SAdS black holes. The dashed line describes $\frac{Re(\omega)(n)}{r_+}$ and the solid line is $\frac{Im(\omega)(n)}{r_+}$. The behave of the QNMs can be expressed as $\frac{\omega(n)}{r_+} \sim (1.385 - 2.220i)n + 2.04 - 1.50i$.

TABLE III: Quasinormal frequencies corresponding to $\lambda = 1$ Dirac perturbation of an intermediate SAdS black hole ($r_+ = 1$).

n	Re(ω)	-Im(ω)	n	Re(ω)	-Im(ω)
0	2.82189	1.28361	6	15.0891	15.0280
1	4.93748	3.51822	7	17.0922	17.3505
2	7.00231	5.79451	8	19.0915	19.6761
3	9.04161	8.08963	9	21.0877	22.0041
4	11.0661	10.3958	10	23.0813	24.3341
5	13.0810	12.7093			

with an error of about 2%, and a spacing is given by

$$\frac{\omega_{(n+1)} - \omega_{(n)}}{r_+} = (2.02 - 2.32i). \quad (4.7)$$

D. Quasinormal Modes for small black hole

We show in Table (IV) and Fig. (6) some of the quasinormal frequencies corresponding to $\lambda = 1$ Dirac perturbation of a small black hole ($r_+ = 0.4$). It is shown that the points for each overtone modes continue to lie along the straight lines $\frac{Re(\omega(n))}{r_+} = 4.18n + 5.45$ and $\frac{Im(\omega(n))}{r_+} = -(2.48n + 0.20)$. That is to say, the behave of the QNMs can be written as

$$\frac{\omega(n)}{r_+} \sim (4.18 - 2.48i)n + (5.45 - 0.20i) \quad (4.8)$$

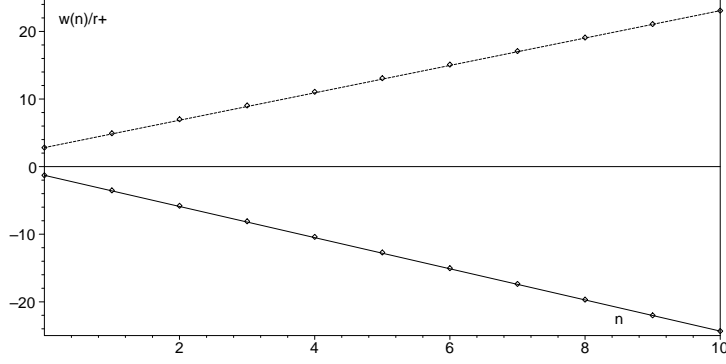


FIG. 5: $\frac{\omega(n)}{r_+}$ versus overtone number n for an intermediate SAdS black hole ($r_+ = 1$). The dashed line describes $\frac{\text{Re}(\omega)(n)}{r_+}$ and the solid line is $\frac{\text{Im}(\omega)(n)}{r_+}$. The behavior of the QNMs can be expressed as $\frac{\omega(n)}{r_+} \sim (2.026 - 2.298i)n + 2.86 - 1.26i$.

TABLE IV: Quasinormal frequencies corresponding to $\lambda = 1$ Dirac perturbation of a small SAdS black hole ($r_+ = 0.4$).

n	$\text{Re}(\omega)$	$-\text{Im}(\omega)$	n	$\text{Re}(\omega)$	$-\text{Im}(\omega)$
0	2.20450	0.17410	6	12.1661	6.03911
1	3.82877	1.07155	7	13.8347	7.05100
2	5.49009	2.03977	8	15.5029	8.06532
3	7.15804	3.02782	9	17.1704	9.08144
4	8.82745	4.02598	10	18.8418	10.0941
5	10.4969	5.03039			

with an error of about 1% except $\omega(0)/r_+$, and a spacing is shown by

$$\frac{\omega_{(n+1)} - \omega_{(n)}}{r_+} = (4.18 - 2.48i). \quad (4.9)$$

V. SUMMARY

The wave equations for the Dirac fields in the SAdS black hole spacetime are obtained by means of the Newman-Penrose formalism. Then, the quasinormal frequencies corresponding to the Dirac field perturbation in the SAdS black hole spacetime are evaluated by using Horowitz-Hubeny approach and the results are presented by tables and figures. We learn from the tables and figures that: (i) For large black holes, both the real and the imaginary parts of the

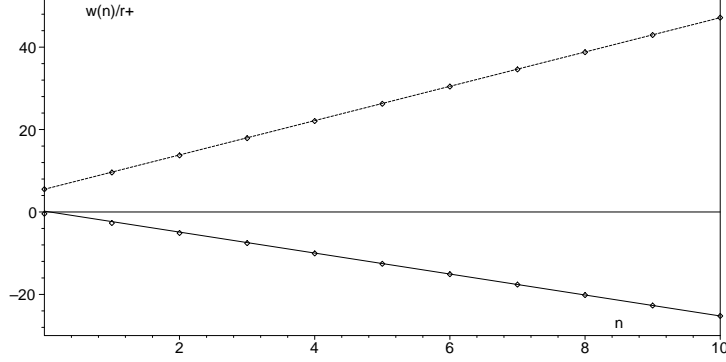


FIG. 6: $\frac{\omega(n)}{r_+}$ versus overtone number n for a small SAdS black hole ($r_+ = 0.4$). The dashed line describes $\frac{Re(\omega)(n)}{r_+}$ and the solid line is $\frac{Im(\omega)(n)}{r_+}$. The behave of the QNMs can be expressed as $\frac{\omega(n)}{r_+} \sim (4.18 - 2.48i)n + 5.45 - 0.20i$.

fundamental quasinormal frequencies are linear functions of the Hawking temperature, and the lines are described by $Re(\omega) = 8.367T$, and $-Im(\omega) = 6.371T$, respectively. For intermediate and small size black holes, $Re(\omega)$ of the fundamental quasinormal frequencies approximates the temperature T more closely than the black hole size r_+ , and $Im(\omega)$ continue to lie along a straight line $-Im(\omega) = 1.499r_+$. (ii) For large black holes (say $r_+ = 100$), the fundamental quasinormal frequencies depend very weakly on the low angular quantum number (say $l = 3/2$ and $l = 5/2$). However, for intermediate and small black holes, the angular quantum number l mode has the surprising effect of increasing the damping time scale (decreasing $|Im(\omega)|$) and decreasing the oscillation time scale (increasing $Re(\omega)$). (iii) For large black holes, an intermediate black hole ($r_+ = 1$) and a small black hole ($r_+ = 0.4$), the behave of the QNMs can be expressed as $\frac{\omega(n)}{r_+} \sim (1.35 - 2.25i)n + (2.136 - 1.500i)$, $\frac{\omega(n)}{r_+} \sim (2.02 - 2.32i)n + (2.86 - 1.26i)$ and $\frac{\omega(n)}{r_+} \sim (4.18 - 2.48i)n + (5.45 - 0.20i)$, respectively, which show that all the modes are evenly spaced, and the smaller the black hole, the larger the spacing.

Acknowledgments

This work was supported by the National Natural Science Foundation of China under Grant No. 10275024 and under Grant No. 10473004; the FANEDD under Grant No. 200317; and the SRFDP under Grant No. 20040542003.

[1] S. Chandrasekhar and S. Detweiler, Proc. R. Soc. Lond. **A 344**, 441 (1975).

- [2] S. Hod, Phys. Rev. Lett. **81**, 4293 (1998).
- [3] O. Dreyer, Phys. Rev. Lett. **90**, 081301 (2003).
- [4] J. Baez, in Matters of gravity. ed. J. Pullin, p. 12(Springer, 2003), gr-qc/0303027.
- [5] G. Kunstatter, gr-qc/0212014; L. Motl, gr-qc/0212096; A. Corichi, gr-qc/0212126; L. Motl and A. Neitzke, hep-th/03301173; A. Maassen van den Brink, gr-qc/0303095.
- [6] J. Maldacena, Adv. Theor. Math. Phys. **2**, 231 (1998).
- [7] E. Witten, Adv. Theor. Math. Phys. **2**, 253 (1998).
- [8] S. Kalyana Rama and Sathiapalan, Mod Phys. Lett. A **14**, 2635 (1999).
- [9] J. S. F. Chan and R. B. Mann, Phys. Rev. D **55** 7546 (1997).
- [10] D. Birmingham, I. Sachs, and S. N. Solodukhin, Phys. Rev. Lett. **88** 151301 (2002).
- [11] V. Cardoso and J. P. S. Lemos, Phys. Rev. D **63** 124015 (2001).
- [12] R. A. Konoplya, Phys. Rev. D **66** 084007 (2002).
- [13] A. O. Starinets, Phys. Rev. D **66** 124013 (2002).
- [14] G. T. Horowitz and V. E. Hubeny, Phys. Rev. D **62** 024027 (2000).
- [15] Y. Kurita and M. A. Sakagami, Phys. Rev. D **67** 024003 (2003).
- [16] V. Cardoso and J. P. S. Lemos, Phys. Rev. D **64** 084017 (2001).
- [17] V. Cardoso, R. Konoplya, and J. P. S. Lemos, gr-qc/0305037.
- [18] R. A. Konoplya, Phys. Rev. D **66** 044009 (2002).
- [19] D. N. Page, Phys. Rev. D **14**, 1509 (1976).
- [20] E. Newman and R. Penrose, J. Math. Phys. (N. Y.) **3**, 566 (1962).
- [21] E. W. Leaver, Phys. Rev. D **34**, 384 (1986).
- [22] K. D. Kokkotas, Class. Quantum Grav. **8**, 2217 (1991).
- [23] H. T. Cho, Phys. Rev. D **68**, 024003 (2003).
- [24] L. Simone and C. M. Will, class. Quantum Grav. **9**, 963 (1992).
- [25] Jiliang Jing, Phys. Rev. D **69**, 084009 (2004).
- [26] Jiliang Jing, Phys. Rev. D **70**, 065004 (2004).